Proceedings World Geothermal Congress 2020+1
Reykjavik, Iceland, April - October 2021

Friction and Wear Behaviour of Surface Coatings for Geothermal Applications

Gifty Oppong Boakye[1], Danyil Kovalov[1,2], Andri Í. Thórhallsson[1], Sigrún N. Karlsdóttir[1], Vlad Motoiu[3]

[1]University of Iceland, Faculty of Industrial Eng., Mechanical Eng., and Computer Science, Hjardarhagi 2-6, Reykjavík, Iceland

[2]Volodymyr Dahl East Ukrainian National University, Severodonetsk, 93400, Ukraine

[3]Tehnoid Com Srl, Bucharest, Romania

gob13@hi.is, dankov@hi.is, ath196@hi.is, snk@hi.is, vladmotoiu@gmail.com

Keywords: Cermets, Coatings, Friction, Geothermal, Sliding, Wear.

ABSTRACT

The global chase for renewable and green energy has led to an increased requirement in geothermal power generation. In such regard, one of the key elements for higher well output and increased efficiency of geothermal turbines and equipment during production is the reduction in mechanical energy loss. The reliability of mechanical systems owing to tribological properties of materials alleviates the negative impact of energy loss from friction and wear. Though desirable friction provides traction to support the motion of mechanical components, when in excess it can lead to unsteady vibrations causing fatigue, cracks, and wear. These damages give rise to production losses through complete loss of component functionality due to changes in the material property. Such tribological issues are observed in entire regions of geothermal power generation cycles; specific problem areas include wellheads, valves, pumps, and the steam turbines. To address these issues, several studies have focused on the development of coating materials as protection against such damages. This study aims to investigate the tribological properties of coatings deposited on substrates that are representatives of geothermal plant components. For this reason, dry sliding experiments were performed on Cermet coated and uncoated flat stainless steel substrates against a tungsten carbide (WC) ball. HVOF coated steels performed much better than bulk 304L and 630 stainless steel substrates. The coatings had a lower coefficient of friction and wear volume. This is due to the coating abrasive resistant microstructure and the dominance of coating-to-metal (WC) contact during the experimental conditions. Microscopic examinations of the wear tracks identified abrasion as the wear mechanism in the stainless steels. The wear track of the coatings showed thin material removal and splat formation for the highly worn-out coating.

1. INTRODUCTION

Large configurations of the power plant are normally multi-stage constructed, machined and assembled into a unit. Assembled components make contact, and an interface is established between the parts. The interactions at the interface during operation are liable to surface damage at certain locations, demonstrated as sliding, pitting or fretting wear that often cause reduction in the component life. In the geothermal field, this will be due to stringent axial, reciprocating and rotary motions, cyclic thermal stresses, and mechanical loads of operation. In addition, the harsh nature; high temperature and chemical composition, of the geothermal steam renders components mechanically vulnerable after long use. In practical life applications, wear is inevitable when surfaces are in contact and in relative motion. The principal cause of wear is friction due to surface finish. However, the two phenomena may be recursive for a sliding couple, since high friction promotes wear and the progression of wear affects friction due to alteration in the contact zone during the wear mechanism (Blau, 2009).

Risk analysis to anticipate failures of a geothermal power plant using failure mode and effect analysis (FMEA) technique identified common damage areas in the steam gathering and transmission equipment, and the turbine and its auxiliary unit. The principal damages compiled in a technical report by Geo-coat project (Fanicchia et al. 2019) from a survey on 12 power plants located world wide yielded similar outcome to the analysis by Feili et al. (Feili et al., 2013). Some typical surface damages were rubbing wear of labyrinth seals, abrasive wear of valves, pump shaft and impellers and wear of turbine rotor due to vibration and imbalances. There are different and various potential solutions to addressing this problem. One of them involves surface texturing of high-grade wear resistant alloys to moderate and optimize surface roughness to control friction. Comprehensive analysis of the effect of surface-topography-texturing on coefficient of friction (CoF) has been performed. Despite excellent contributions that have been made by surface texturing under lubricated conditions (Menezes, 2016; Gachot et al., 2017), some researches have documented unsuccessful cases under dry conditions. Saha et al. (Saha et al., 1996) studied the influence of surface topography on frictional behaviour of AA 3104 Aluminium sheet. The CoF increased with strain and the analysis supported Archard's model (Archard, 1953) of flattening of surface asperities to increase the real area of contact and wear volume. Menezes reported high CoF values and volume loss on laser textured SAE 1035 steel under dry conditions in comparison to the lubricated surface that experienced less shear action (Menezes, 2016). The high CoF evolution are logically interpreted by an article published by Kang et al., that clearly revealed the contribution of adhesion on surface textured materials under dry sliding conditions (Kang et al. 2015). Kang concluded that the dry sliding of micro-domed and nano-dimpled aluminium substrates increased lateral contact (at small points and angles) and material-couple sticking due to interlocking influencing frictional force.

Another potential solution to increase wear resistance is the addition of a thin protective layer to the component surfaces. The merit is that the layer does not necessarily have to alter the component properties neither participate in the structural application. Currently, metallic-carbide matrix coatings with several elements (often; Ni, Co, Cr, W, Fe, B, Mo) (Mannem et al., 2008) are deposited on hydro and geothermal turbine components (Sakai et al., 2005; Shiokawa, and Kunio 2005; Mann and Arya 2001) to improve friction, wear and corrosion resistance (Mann and Arya, 2001; Sidhu et al., 2010; Bolelli et al., 2012). However, coatings are not used as a standard practice but only limited to parts of the turbine such as the tip of blades and reports are more common for clean steam and hydropower turbines, therefore, the need for further studies. Deposition on blades is normally by brazing or

welding, but there are numerous problems associated with the use of precursor materials or application methods. Thus, the deposition is limited to thermal spraying due to decarburization of carbide and HVOF method has been reported as an excellent deposition technique (Guo et al., 2011). In spite of the reported friction and wear advantages of thermally sprayed coatings some drawbacks have been identified. Wood observed low fracture toughness of WC coating systems tested under dry sliding condition and reported the susceptibility of the coating to crack initiation and propagation due to the microstructure (Wood, 2010). However, bond coatings such as NiCr applied with Cr_3C_2 and Co/CoCr deposited prior to WC systems have been reported to improve adhesion and strengthen the matrix (Lima and Guilemany, 2007). In another article, HVOF sprayed WC-Co-Cr coating was tested in a corrosive environment and the corrosion resistance was attributed to Cr and the formation of chromium oxide (Souza and Neville, 2006). Therefore, several researchers have studied the mechanical performance of chromium-based Cermet coatings. These wear resistant coatings are based on metallic phase, such as nickel or iron alloys, along with a chromium carbide ceramic phase. A dry wear test of Cr_xC_y-NiCr coatings at load range 63-75 N recorded low abrasive wear behaviour. The X-ray diffraction result from the experiment also revealed the appearance of chromium oxide (Cr_2O_3) amongst others on the surfaces (Wirojanupatump et al., 2001). Ni-based Cermet alloy has also been reported to enhance wear and corrosion resistance in engineering applications even for high-temperature purposes (Bolelli et al., 2012).

The present work, therefore, focuses on testing tribological properties, friction and wear, of Cermet coatings deposited on substrates that are representatives of geothermal plant components. Friction coefficient and wear volume of three different HVOF sprayed Cermet coatings; WC-Co-Cr (CA1) Cr_3C_2–NiCr (CA2) and a Ni-Cr-Fe-Si-B-C alloy (CA3), were measured under dry sliding conditions. As terms of comparison, two stainless steels were also tested.

2. MATERIALS AND METHODS

Stainless steels are used for geothermal plant components due to their known corrosion and wear resistance. As such, the powders were thermally sprayed onto 316L stainless steel substrates. The coated disc had 50mm-diameter x 6mm-thickness disc and an M6 threaded hole required for handling during the deposition process. The coatings were produced by Tehnoid Com Srl (Bucharest, Romania) using high velocity oxy-fuel (HVOF) technique. Three different coated materials were tested against a WC ball, namely; WC-Co-Cr (CA1), Cr_3C_2–NiCr (CA2) and a Ni-Cr-Fe-Si-B-C alloy (CA3). The feedstock, production process and final composition of the coatings are described in Table 1. Scanning electron microscopy (SEM) was used to characterise the various features of the deposited coatings before and after tribological tests.

Table 1: The feedstock, production process and final composition of the coatings

Commercial name	**Process involved**	**Composition** (wt. %)					
(a) **CA1** WC-Co-Cr	Sintering and crushing	5.3**C**	10**Co**	4**Cr**	Bal **_W**		
(b) **CA2** Cr_3C_2–NiCr	Agglomeration and plasma densification	9.5**C**	20**Ni**	Bal **_Cr**			
(c) **CA3** Ni-Cr-Fe-Si-B-C	Gas atomisation	1.0**C**	3.5**B**	17**Cr**	4**Fe**	4**Si**	Bal **_Ni**

Table 2: Chemical composition of bulk 304L and 630 stainless steels used in the dry sliding test

Chemical composition (S1 -304L SS)									
Weight %	**C**	**Mn**	**P**	**S**	**Si**	**Ni**	**Cr**	**Al**	**Sn**
Average	0.035	2	0.045	0.03	1	10	19	6	4
Chemical composition (S2 -630 SS)									
Weight %	**C**	**Mn**	**P**	**S**	**Si**	**Ni**	**Cr**	**Cu**	**Na+Ta**
Average	0.07	1	0.04	0.03	1	4	16.5	4	0.3

3. EXPERIMENTAL DETAILS

The sliding wear tests were conducted with a ball-on-disc configuration using Anton Paar® tribometer under ambient laboratory environment. The set-up and measurements were in accordance to ASTM G99 standard (ASTM G99-05, 2011). The unlubricated (i.e., dry) test involved unidirectional sliding of a ball pressed against each coated/uncoated metallic surface at an applied load to generate friction, illustrated schematically in Figure 1. The rubbing counterpart was a tungsten carbide (WC) ball of 6mm diameter. A different ball was used for each test and repetitions. Prior to the tribological test, the working areas of the uncoated samples were mechanically polished to a mirror finish using silicon carbide papers to 2400 grit size. After wet grinding, the samples were cleaned with deionized water, acetone and air-dried, whereas, the coatings were tested ‘as-deposited’. Average roughness (Ra) were determined in six different locations of each sample and the results were averaged. For all cases the applied load was 5N, the test duration and motor speed were kept constant at 3600 sec and 200 rpm respectively. The sequential test procedure is described in Table 3. Considering the variation in radius, the corresponding linear velocities, sliding distances, and other test parameters are summarized in Table 4.

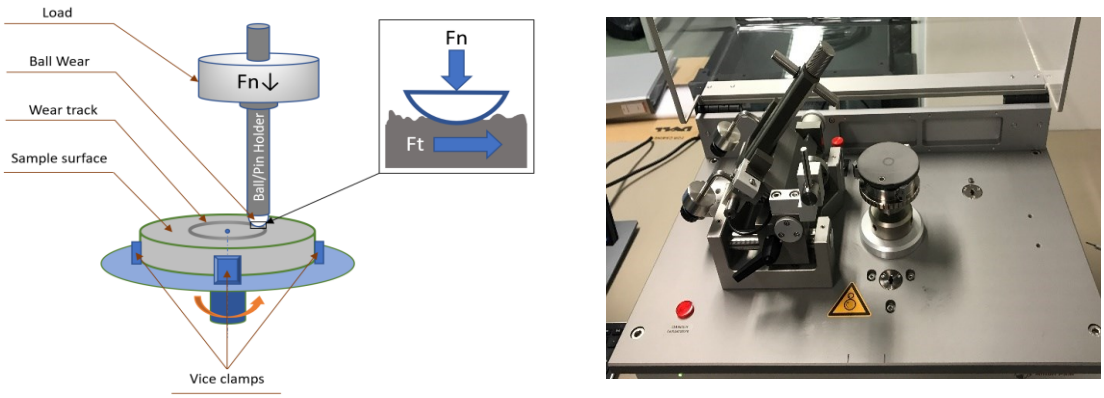

(a) (b)

Figure 1: Schematic illustration of pin-on-disk sliding test and image of tribometer used in the wear test.

Table 3: The sequential test procedure used in the dry sliding wear test

Steps	***Experiment Description***	***Information of interest***
1. Sample Cleaning	Cleaning to remove all dirt and foreign materials	Good surface finish, Roughness and hardness measurements.
2. Mounting the setup	Insert the ball in holder, secure the disc on the stage, make contact and adjust desired conditions.	Conditions for measurable wear: Load (F_n), Motor speed, Track radius, Distance / Cycles, Environment, Rubbing time.
3. Begin test under selected load.	Add load (N) and initiate sliding motion with time.	Generation of the Tangential force (F_t) Coefficient of friction (μ) and wear track.
4. End test and remove sample	Test stops after selected revolution and repeated twice. Sample is removed and then examined.	Discoloration, Visible distorted features, wear scar (SEM)

Table 4: The linear velocities, sliding distances and other test parameters used in the dry sliding wear test.

Material	**Test**	**Load (N)**	**Track Radius (mm)**	**Sliding speed (m/s)**	**Sliding distance (m)**	**No. of cycles (*10^3)**	**Time (sec)**
S1 – S2	1	5	5	1.10	377	12	3600
	2		8	1.70	603	12	3600
	3		11	2.30	830	12	3600
HVOF-CERMET	1	5	10	2.10	754	12	3600
	2		13	2.70	980	12	3600
	3		16	3.40	1206	12	3600

The coefficient of friction was monitored during rubbing without interruption. The evolution of the coefficient of friction (CoF) was plotted as a function of time for all the tribological pairs. Also, the average coefficient of friction, μ, was determined using the equation (ASTM G99-05 2011):

$$\mu = \frac{F_t}{F_n} \quad (1)$$

where F_n, F_t, *[N]* are the applied or normal force, and the tangential force, respectively.

The wear volume was calculated by multiplying the average transversal area by the circumference of the track obtained from an optical profilometer

$$V = A \cdot d\ [mm^3] \quad (2)$$

where A [mm^2], d[mm], are transversal area, circumference of the track, respectively.

Considering the micro-contact of surfaces during the interfacial sliding, wear is reported to result from energy dissipation between the mechanical pair. Friction, therefore, plays a crucial role. The total energy dissipated (E_d) during the test was calculated from (Huq and Celis, 2002):

$$E_d = F_t \cdot d = \mu \cdot F_n \cdot v \cdot t \quad (3)$$

where μ, v (m/s), F_n (N), t (sec), are cumulative friction, velocity, normal force, time respectively.

4. RESULTS AND DISCUSSION

SEM was used to observe the morphology of the deposited coatings (Fig. 2) and the bulk substrates (see Section 4.3). The micrographs in Figure 2 show the microstructure of the coatings after deposition and before pin-on-disk testing. In the image, the Cermet coatings appear to be dense, low porosity, and crack free. The thickness of the coatings estimated using microscopy was in the range of 130-145 µm. The coatings had an average surface roughness (Ra) of approximately 9.1±0.5 µm while the bulk substrates had a Ra -0.1±0.02 µm.

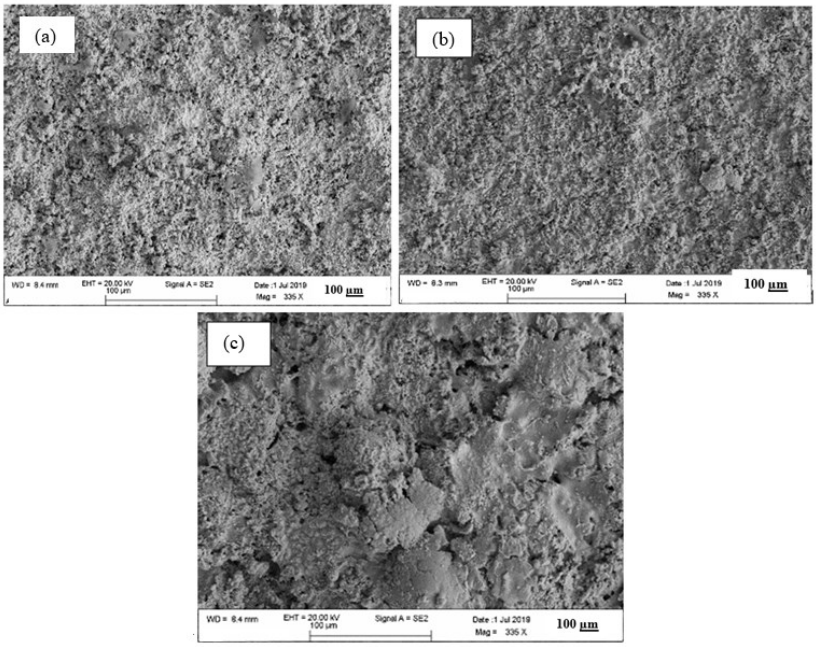

Figure 3: SEM micrographs showing the morphology of the HVOF (a) CA1 – WC-Co-Cr Cermet, (b) Cr_3C_2-NiCr Cermet and (c) CA3 – Ni-Cr-Fe-Si-B-C Cermets.

4.1 Evolution of the coefficient of friction

Figure 3 shows the effect of the applied force on the sliding coefficient of friction of the tested materials against WC. After the onset of sliding, two regions; the running-in and the steady state were apparent for all the opposing surface pairs with different behaviour for each pair of materials under the test conditions. This is similar to most reported works (Bolelli et al. 2012). In most cases of repetitive testing, the starting CoF was negative, below -0.1. This suggests possibly a nanometric scale atomic interaction at the interface of the surfaces at close contact. During the run-in stage, the CoF rises rapidly until a critical value is attained. Once the level was reached, the CoF was observed to maintain a steady state over the specific test distance or time. At such point, a transition from static contact to sliding contact between the two surfaces is achieved. The run-in process was accompanied by high energy dissipation to support the sliding due to the small initial contact points at the interface from the surface topography of the matched samples. The phenomenon involved surface wear of the highest points or peaks called asperities within the contact, from which the real contact area arose. Thus, the initial rise in friction is explained to result from the smearing-off of the highest contacting peaks to improve the load bearing characteristics at the surface by increasing the actual/real contact area (observed during the steady state).

At the same load condition for the bulk metals; S1 and S2; a similar behaviour of CoF evolution with sliding time was seen. The friction coefficient at the initial stages of sliding showed a lower stability, then after 1000 sec, an oscillating steady state behaviour was observed. After run-in, both curves rapidly increased to a maximum CoF value (0.8-0.9) before the steady state condition was reached. However, 304L experienced run-in at a lower friction value (0.45), but transition into steady state was much slower. Obviously, the trend shows that the state of the friction contact at the interface changed over the entire duration for both steels. The high initial CoF value arose from increased plastic deformation (i.e., permanent damage) of the asperities between the WC and the flat stainless steels. The surface damage can be interpreted in terms of the initial stages where the hard WC ball wears-through the thin films on the stainless steels. The wear then resulted in gradual generation and accumulation of the wear particles (debris). On the contrary, debris generation in WC-630 SS pair can be said to be abrupt due to high run-in CoF value and a comparatively faster steady state transition (Fig. 3b).

In the HVOF Cermet coated samples, it was observed that the run-in was at lower friction values (0.3-0.65). In addition to achieving steady state at a faster rate (100 sec), the tangential force declines compared to the stainless steels. CA2 and CA3 had similar curve behaviour where running-in blends with the steady state-region. This may be attributed to the smearing or wearing of high surface asperities as compared to the wear-through observed in the steels. Thus, both CoF curves suggest the removal of a thin

film from the surface for the entire test duration. After 2500 sec, CA3 observed a slight rise in CoF (Fig. 3a) comparatively to CA2 which could be explained as further wear with subsequent debris formation. In other cases, the initial worn thin film is likely acting as a lubricating layer due to entrapment and size reduction. The distinct feature is prominent in the CoF curve of CA1 after running-in. The transfer layer transitioned the sliding system to a low friction system. Similar range of CoF values under dry sliding were observed for the same composition of HVOF sprayed commercial powders of WC-Co-Cr (CA1), Cr_3C_2–NiCr (CA2) and Ni-Cr-Fe-Si-B-C (CA3) reported by Wood (Wood, 2010), Bolelli et al. (Bolelli et al., 2012) and Kekes et al. (Kekes et al., 2014) respectively.

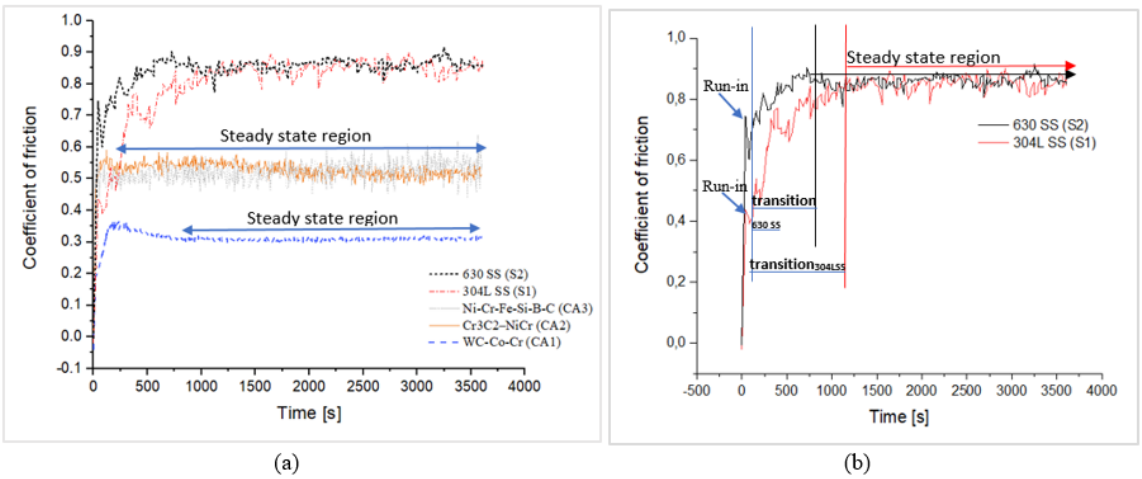

Figure 4: Graphs of the CoF (μ) vs. time (sec) (a) of tested materials and (b) of the stainless steels showing the effect of the applied force and sliding on the evolution of the coefficient of friction.

4.2 Friction reduction and energy dissipation

Figure 4 shows the reduction in coefficient of friction due to the application of the Cermet coatings. This indicates that decreased contact and penetration of metallic surfaces during sliding could be achieved for components in geothermal environment with application of these coatings by reducing the friction and wear. Thus, Figure 4 shows the extent of CoF reduction by the Cermet coatings. The average CoF during sliding of tested materials under the same load is presented. In general, frictional forces were at a minimum in the HVOF Cermet coated samples. The energy (kJ) acquired was positive, but the negative axis presented in Figure 5(b) depicts that, this energy was not invested in useful work. It can be seen that samples with the highest CoF (0.5-0.84) had higher energy dissipation.

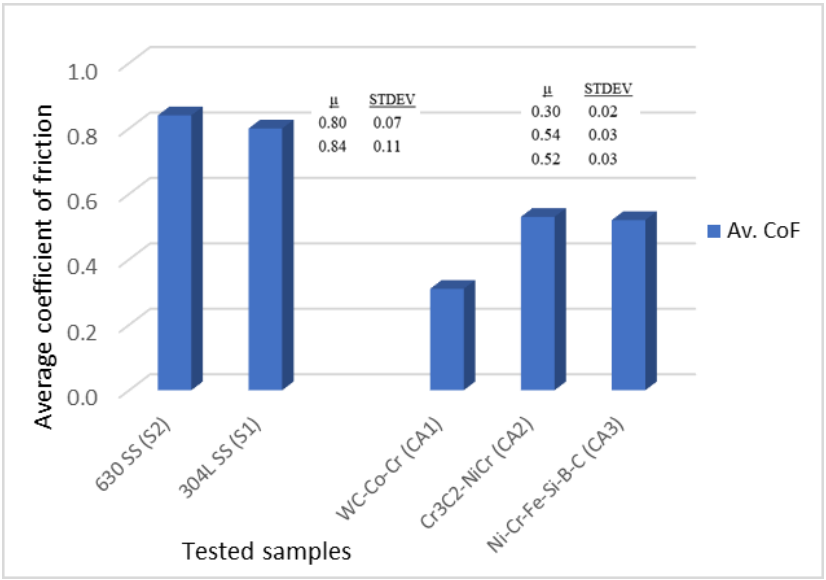

Figure 5: Graph showing the average coefficient of friction for all tested materials under the dry sliding test.

The energy dissipated is a function of the cumulative frictional force, the applied load, the velocity, and time (Eq. 3). Figure 5a shows a higher dependence of the energy dissipated on the frictional force and the velocity. This is because, for an applied force, the resulting tangential force is a fraction of the applied force that produces undesirable work. For instance, in the WC-stainless steels pair, 4/5th of the applied load was directed towards non-useful energy such as friction rather than the sliding. During the sliding experiment, other forms of such energy were observed as noise, heat, and vibration. However, it is interesting to mention, even for wear test performed at higher velocities for the

coatings, the coating showing the least improved performance; CA3 halved the force retarding or impeding motion between the surface pairs.

Each test was repeated three times and the average results were as shown in Table 5. Figure 5a shows a good linear relationship between the wear volume and the dissipated energy from which the energy wear rate was calculated; as the slope of the linear evolution of the wear volume. In fact, the linear behaviour has been demonstrated by Huq and Celis in a dry sliding experiment (Huq and Celis, 2002). The lower correlation of S1 and S2 is because in all of the tests, the substrates were penetrated, resulting in chunk material removal (Fig. 5b) wherein the wear losses affect the tribo-system. The total volume of material lost at the surface of each sample was calculated and presented in Figure 5b together with energy dissipated during sliding at the constant load condition. The highest wear volume corresponds to the highest energy dissipated and the highest CoF value in Figure 4. Therefore, in this study, the volume of material removed from the surface was observed to be proportional to the energy dissipated by the friction. No significant wear was observed on the WC balls in sliding contact with the Cermet coatings under an optical microscope. However, a scar was observed for WC-on-stainless steel wear test.

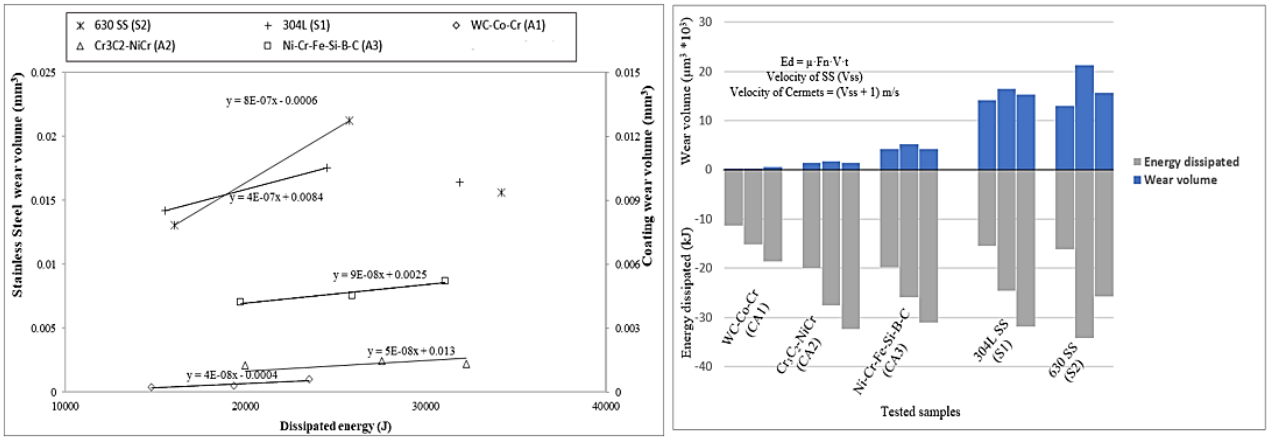

(a) (b)

Figure 6: Graph of showing (a) the wear volume (mm3) vs. dissipated energy (J), (b) the total volume of material lost and the energy dissipated (kJ) at the surface of each sample.

Table 5: Average values of friction and the wear volume obtained for at an average speed of 1.7 m/s (Stainless Steels) and 2.7 m/s (Cermet coatings)

Materials / Pin - Disk	Average wear volume (mm^3)	Energy wear rate (mm^3/J)	Average friction
WC - WC-Co-Cr	3.8×10^{-4}	4.0×10^{-8}	0.30
WC - Cr_3C_2–NiCr	1.5×10^{-3}	5.0×10^{-8}	0.54
WC - Ni-Cr-Fe-Si-B-C	4.5×10^{-3}	9.0×10^{-8}	0.52
WC - 304L SS	1.6×10^{-2}	4.0×10^{-7}	0.80
WC - 630 SS	1.7×10^{-2}	8.0×10^{-7}	0.84

4.3 Sliding wear morphology

The average results given above show that the Cermet coatings improved the wear behaviour of the substrate steel. This was because substrate indentation was prevented, and coating-to-metallic contact was dominant within the sliding process. The wear tracks were investigated using a scanning electron microscope (SEM) to understand the phenomenon of wear. Figure 6 shows SEM micrographs of Cermet coated and stainless steel materials used; tested and non-tested. The predominant mechanism observed for the stainless steels samples S1 and S2 was abrasive wear. The abrasive wear is characterized by ridge-in-groove type straitions in the direction of the sliding. Similar to the friction curve, the evolution of wear in the initial stages arouse from groove ploughing and microcutting seen prevalent in the micrographs under lower magnification.

In the wear behaviour of the Cermet coatings, no detachment or pull outs were observed. The SEM micrographs of samples CA1, CA2 showed only smearing and removal of a thin layer of coating (Fig 6a). The wear behaviour follows Archard´s contact model (Archard 1953) wherein the highest peaks on the surfaces smear-off to enhance asperity contact. However, CA3 experienced comparatively higher wear and the formation of splats (Fig. 6a). At higher magnification (Fig. 7), the micro-wear features of the splat in CA3 structured coating exhibited a smooth surface, slight abrasive scratch lines, and microchips. Microchipping was a mild wear mechanism responsible for thin and continuous debris formation on the sample. In Figure 7, there is evidence of deformation and material removal presented as loose wear particles on the surface of the sample. This accounts for the slight friction rise observed in the CoF steady state condition curve and high energy dissipation.

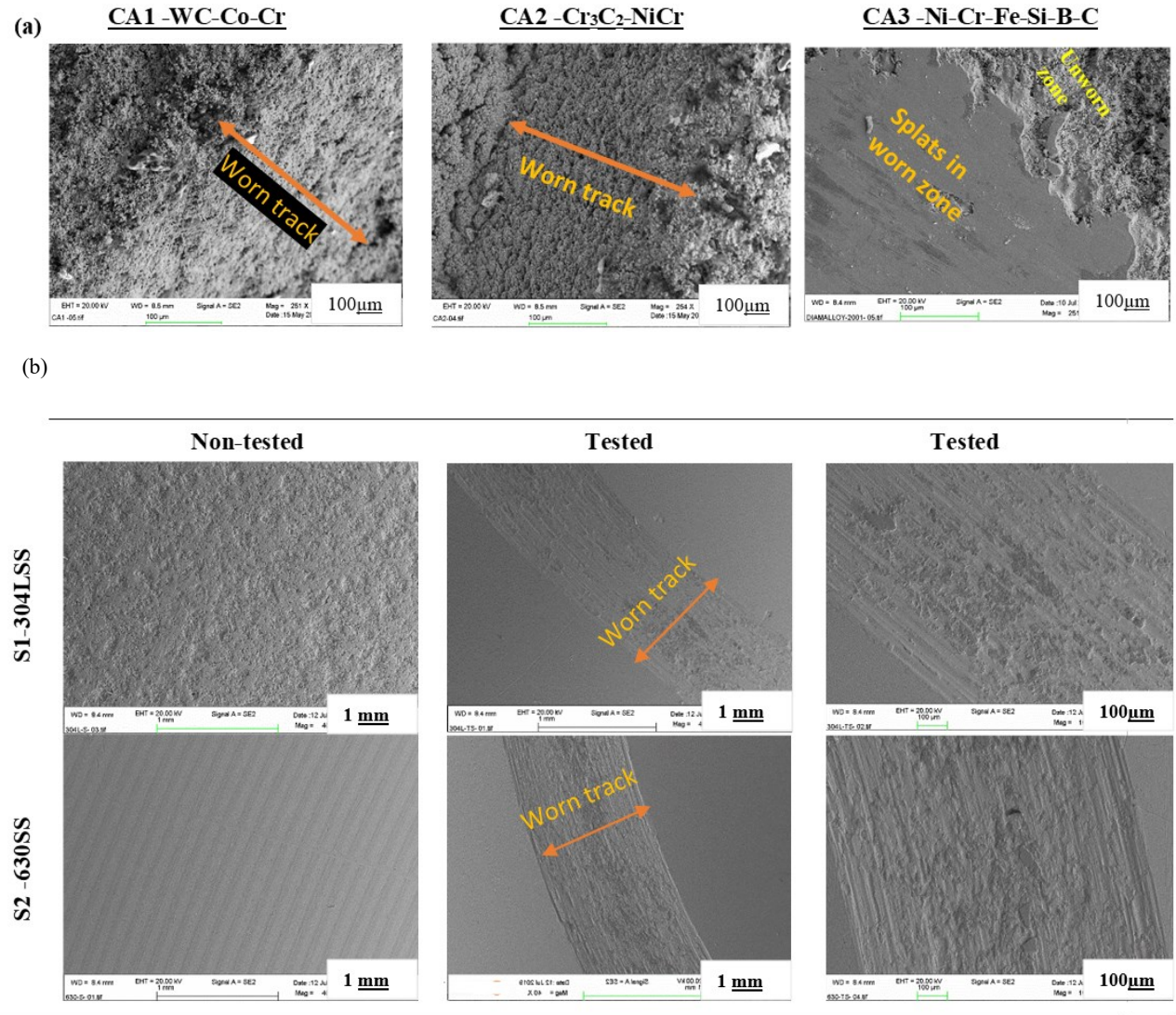

Figure 7: The SEM micrographs of (a) tested HVOF Cermet coatings and (b) tested and non-tested stainless steel materials used in the pin-on-disk test.

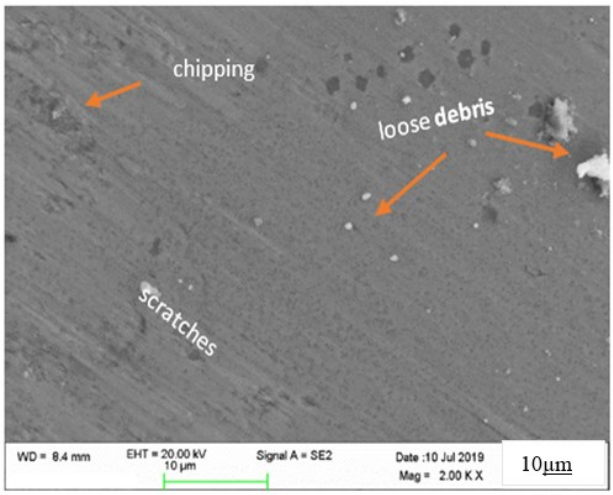

Figure 7: The SEM micrograph showing worn surface of CA3- Ni-Cr-Fe-Si-B-C after dry sliding wear test.

Likewise, at higher magnification, deeper scratches, chipping and wear particles were visible on the stainless steel samples (Fig. 8). The SEM micrograph of 304 L shows abrasive and adhesion wear mechanism. The main wear features were microcutting and microchips which formed thin continuous ridges and debris (Fig 8a). Fragmented debris particles were formed due to gradual delamination within the contact area and continuous sliding. Thus, delaminative wear on the steel resulted in zones characterised by accumulated and adhered wear particles (Fig 8b). This confirms that, the high CoF was associated with the digging-in of the WC ball, as the wear track width increases with pull-outs, forming surface craters. This process had a significant effect on the volume of material loss. However, the entrapped particles built up between the contact and upon further size reduction of the adhered surface film was sufficient enough to sustain the applied force. This is the reason for a lower CoF, and volume loss in 304L compared to 630 SS. The SEM micrograph of 630 SS (usually used as a blade material in geothermal plants) was characterized by severe plastic deformation. The main wear feature was microploughing forming deeper ridges and a rougher surface. The debris generated was discontinuous, thick, and loosely attached to the surface. As such, 630 SS had the highest wear volume and energy dissipation following the high friction force.

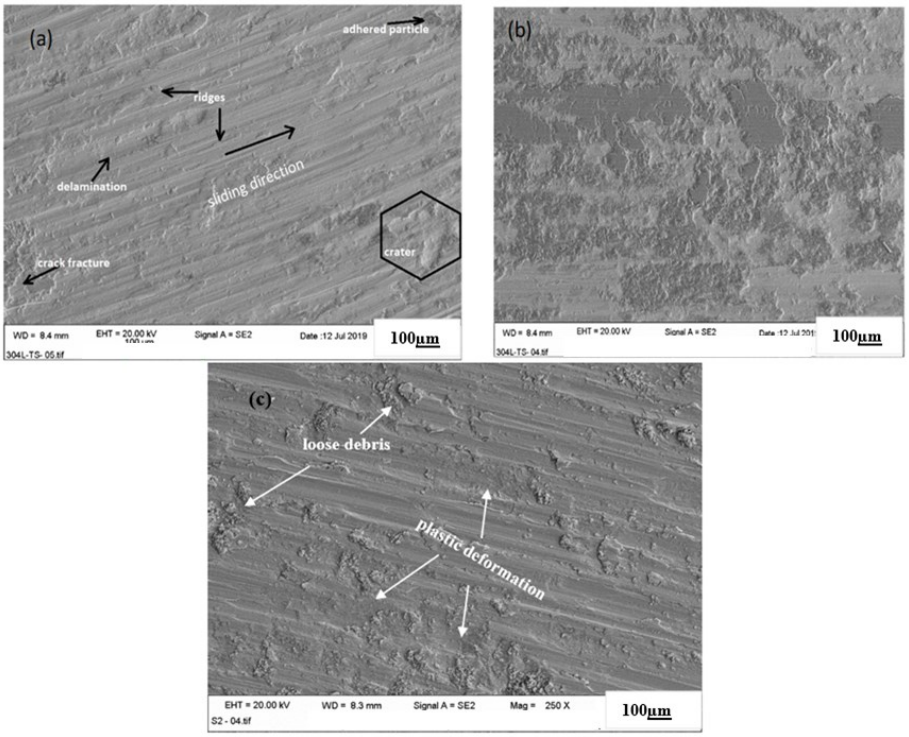

Figure 8: SEM micrographs showing worn surface of stainless steel samples; (a), (b) 304L SS and (c) 630 SS after dry sliding wear test.

CONCLUSION.

Pin-on-disk sliding test was successfully used to investigate the friction and wear behaviour of all test samples. The bulk materials; 304 L and 630 SS were observed to have a high coefficient of friction (0.8-0.85) during the sliding test. The rise in the coefficient of friction was observed to accompany high energy dissipation due to permanent damage and material loss, which is required to compensate for the initial sliding condition. On the other hand, the wear mechanism of the HVOF sprayed Cermet coatings had lower CoF values (0.3-0.54), minimum surface damage and no penetration into the substrate material was observed. The dominant wear behaviour observed in the experiment were abrasive wear, delaminative wear and third body interferences due to the accumulation of debris within the contacting interface. The wear behaviour of all the tested materials correlated with the average values from both the evolution of CoF and the calculated worn volume on the sample surfaces. The stainless steel samples had the highest material loss. The coatings exhibited the best performance by serving as a protective surface to resist abrasion.

ACKNOWLEDGEMENT

This work was part of the H2020 EU project Geo-Coat: 'Development of novel and cost-effective corrosion resistant coatings for high-temperature geothermal applications' funded by H2020 EU project no. 764086. The authors would also like to acknowledge the resources and collaborative efforts provided by the consortium of the Geo-Coat project.

REFERENCES

Archard, J. F. 1953. "Contact and Rubbing of Flat Surfaces." *Journal of Applied Physics* 24 (8): 981–88. https://doi.org/10.1063/1.1721448.

ASTM G99-05. 2011. "Standard Test Method for Wear Testing with a Pin-on-Disk Apparatus." *Annual Book of ASTM Standards* 05 (Reapproved 2010): 1–5. https://doi.org/10.1520/G0099-05R10.2.

Blau, P. J. 2009. *Friction Science and Technology: From Concept to Application*. *Society of Tribologists and Lubrication Engineere*. Second edi. London, New York: Taylor & Francis.

Bolelli, Giovanni, Benedetta Bonferroni, Jussi Laurila, Luca Lusvarghi, Andrea Milanti, Kari Niemi, and Petri Vuoristo. 2012. "Micromechanical Properties and Sliding Wear Behaviour of HVOF-Sprayed Fe-Based Alloy Coatings." *Wear* 276–277 (February): 29–47. https://doi.org/10.1016/J.WEAR.2011.12.001.

Fanicchia, Francesco, Frazer Brownlie, Sæmundur Guðlaugsson, Gifty Oppong, Ioana Csaki, Sunna Ó Wallevik, Fahim Chowdhury, Vlad Motoiu, and Per Kjellgren. 2019. "Development of Novel and Cost Effective Corrosion and Erosion Resistant Coatings for Geothermal Steam Turbines." In *10th International Charles Parsons Turbine and Generator Conference*, 11. Cranfield, UK.

Feili, Hamid Reza., Navid. Akar, Hossein. Lotfizadeh, Mohammad. Bairampour, and Sina. Nasiri. 2013. "Risk Analysis of Geothermal Power Plants Using Failure Modes and Effects Analysis (FMEA) Technique." *Energy Conversion and Management* 72 (04): 69–76. https://doi.org/10.1016/j.enconman.2012.10.027.

Gachot, C., A. Rosenkranz, S. M. Hsu, and H. L. Costa. 2017. "A Critical Assessment of Surface Texturing for Friction and Wear Improvement." *Wear*. https://doi.org/10.1016/j.wear.2016.11.020.

Guo, R.Q., C. Zhang, Q. Chen, Y. Yang, N. Li, and L. Liu. 2011. "Study of Structure and Corrosion Resistance of Fe-Based Amorphous Coatings Prepared by HVAF and HVOF." *Corrosion Science* 53 (7): 2351–56. https://doi.org/10.1016/J.CORSCI.2010.12.022.

Huq, M. Z., and J. P. Celis. 2002. "Expressing Wear Rate in Sliding Contacts Based on Dissipated Energy." *Wear* 252 (5–6): 375–83. https://doi.org/10.1016/S0043-1648(01)00867-5.

Kang, Myeong, Y. M. Park, B. H. Kim, and Young Ho Seo. 2015. "Micro- and Nanoscale Surface Texturing Effects on Surface Friction." *Applied Surface Science*. https://doi.org/10.1016/j.apsusc.2015.03.194.

Kekes, D., P. Psyllaki, and M. Vardavoulias. 2014. "Wear Micro-Mechanisms of Composite WC-Co/Cr-NiCrFeBSiC Coatings. Part I: Dry Sliding." *Tribology in Industry* 36 (4): 361–74.

Lima, C.R.C., and J.M. Guilemany. 2007. "Adhesion Improvements of Thermal Barrier Coatings with HVOF Thermally Sprayed Bond Coats." *Surface and Coatings Technology* 201 (8): 4694–4701. https://doi.org/10.1016/J.SURFCOAT.2006.10.005.

Mann, B.S., and V. Arya. 2001. "Abrasive and Erosive Wear Characteristics of Plasma Nitriding and HVOF Coatings: Their Application in Hydro Turbines." *Wear* 249 (5–6): 354–60. https://doi.org/10.1016/S0043-1648(01)00537-3.

Mannem, U. D., K. Anand, D. M. Gray, and F. Ghasripoor. 2008. "Protective Coatings Which Provide Wear Resistance and Low Friction Characteristics, and Related Articles and Methods." US 2008/0145649 A1. https://patents.google.com/patent/US20080145649A1/en.

Menezes, P. L. 2016. "Surface Texturing to Control Friction and Wear for Energy Efficiency and Sustainability." *International Journal of Advanced Manufacturing Technology* 85 (5–8): 1385–94. https://doi.org/10.1007/s00170-015-8058-2.

Saha, Pradip K., William R.D. Wilson, and Roland S. Timsit. 1996. "Influence of Surface Topography on the Frictional Characteristics of 3104 Aluminum Alloy Sheet." *Wear*. https://doi.org/10.1016/0043-1648(95)06881-3.

Sakai, Yoshihiro., Kenji. Shiokawa, and Nakamura. Kunio. 2005. "Recent Technologies for Geothermal Steam Turbine." In *FUJI ELECTRIC REVIEW*, 51:90–95.

Sidhu, H. S., B. S. Sidhu, and S. Prakash. 2010. "Wear Characteristics of Cr3C2–NiCr and WC–Co Coatings Deposited by LPG Fueled HVOF." *Tribology International* 43 (5–6): 887–90. https://doi.org/10.1016/J.TRIBOINT.2009.12.016.

Souza, V. A. D., and A. Neville. 2006. "Mechanisms and Kinetics of WC-Co-Cr High Velocity Oxy-Fuel Thermal Spray Coating Degradation in Corrosive Environments." *Journal of Thermal Spray Technology* 15 (1): 106–17. https://doi.org/10.1361/105996306X92677.

Wirojanupatump, S, P.H Shipway, and D.G McCartney. 2001. "The Influence of HVOF Powder Feedstock Characteristics on the Abrasive Wear Behaviour of CrxCy–NiCr Coatings." *Wear* 249 (9): 829–37. https://doi.org/10.1016/S0043-1648(01)00821-3.

Wood, R.J.K. 2010. "Tribology of Thermal Sprayed WC-Co Coatings." *International Journal of Refractory Metals and Hard Materials* 28 (1): 82–94. https://doi.org/10.1016/j.ijrmhm.2009.07.011.